Annual Review of Condensed Matter Physics

Floquet Engineering of Quantum Materials

Takashi Oka[1,2] and Sota Kitamura[1]

[1]Max Planck Institute for the Physics of Complex Systems, 01187 Dresden, Germany; email: oka@pks.mpg.de, kitamura@pks.mpg.de

[2]Max Planck Institute for Chemical Physics of Solids, 01187 Dresden, Germany

Annu. Rev. Condens. Matter Phys. 2019. 10:387–408

First published as a Review in Advance on December 14, 2018

The *Annual Review of Condensed Matter Physics* is online at conmatphys.annualreviews.org

https://doi.org/10.1146/annurev-conmatphys-031218-013423

Keywords

Floquet topological systems, ultrafast spintronics, Mott insulator, nonequilibrium quantum systems

Abstract

Floquet engineering, the control of quantum systems using periodic driving, is an old concept in condensed matter physics dating back to ideas such as the inverse Faraday effect. However, there is a renewed interest in this concept owing to (*a*) the rapid developments in laser and ultrafast spectroscopy techniques, (*b*) discovery and understanding of various "quantum materials" hosting interesting exotic quantum properties, and (*c*) communication with different areas of physics such as artificial matter and nonequilibrium quantum statistical physics. Here, starting from a nontechnical introduction with emphasis on the Floquet picture and effective Hamiltonians, we review the recent applications of Floquet engineering in ultrafast, nonlinear phenomena in the solid state. In particular, Floquet topological states and their application to ultrafast spintronics and strongly correlated electron systems are overviewed.

1. INTRODUCTION

How fast and drastically can we change electronic properties of materials, and what would be the most efficient way to do this? This is an interesting fundamental question and, at the same time, has connections to the electronic technology that supports our everyday lives. Semiconductor devices surrounding us such as solar cells, transistors, and memories typically involve nonequilibrium processes triggered through light-matter coupling, and the application of electromagnetic fields changes their properties (transport, carrier density, magnetization, etc.) drastically. There is a growing interest in ultrafast (1–13) and nonlinear (14–16) electronics with the aim to find a way to control postsemiconductor materials hosting exotic quantum properties.

Although this research area has a long history, recently there have been some theoretical developments enabling us to understand various phenomena systematically. One powerful tool is the concept of Floquet engineering, i.e., the control of quantum systems using time-periodic external fields. Theoretically, continuous irradiation of a laser can be modeled by a time-periodic perturbation, and the Hamiltonian $H(t)$ describing the irradiated system inherits the time periodicity

$$H(t+T) = H(t), \qquad 1.$$

where the periodicity $T = 2\pi/\Omega$ is related to the photon energy or driving frequency Ω (we set $\hbar = 1$). During the past several decades, with the help of the Floquet theorem (17–20), which is a temporal analog of the Bloch theorem, the understanding of periodically driven systems has advanced considerably especially for open transport problems (21, 22), laser-driven atoms (23), strongly correlated electron systems (9, 24–33), and electron–phonon systems (32, 34–39) and their universal mathematical structures for closed systems (40–48). It is possible to dynamically induce interesting exotic quantum states by carefully selecting the driving laser that matches the target material. Although Floquet engineering is now applied in several fields of physics, most notably in cold atoms in optical traps (49, 50), here, we focus on its application in electronic systems as illustrated in **Figure 1**.

2. BASICS OF FLOQUET ENGINEERING

We consider systems periodically driven by external fields with a Hamiltonian satisfying the periodicity condition (Equation 1). The basic idea of the Floquet method is to expand quantities into Fourier modes $e^{-im\Omega t}$ with $m = 0, \pm 1, \ldots$. The Floquet picture (or Shirley picture) is not only useful in doing systematic calculations but also provides an intuitive way of understanding driven systems (17). In single-body problems, it gives a mapping to a quantum model with one extra dimension. The index m of the Fourier mode can be considered as a lattice site index in a fictitious Floquet direction (**Figure 2**). Let us consider this in more detail.

When the Hamiltonian is time periodic, as in the Bloch theorem, one can take the set of solutions of the time-dependent Schrödinger equation to be a product of a time-periodic function and a nonperiodic phase factor; i.e.,

$$|\Psi(t)\rangle = e^{-i\varepsilon t}|\Phi(t)\rangle, \quad |\Phi(t+T)\rangle = |\Phi(t)\rangle. \qquad 2.$$

The time-periodic function $|\Phi(t)\rangle$ is called the Floquet state, and ε the Floquet quasi-energy. Note that ε has an indefiniteness of integer multiples of Ω. We use the Fourier expansion,

$$H(t) = \sum_m e^{-im\Omega t} H_m, \quad |\Phi(t)\rangle = \sum_m e^{-im\Omega t}|\Phi^m\rangle, \qquad 3.$$

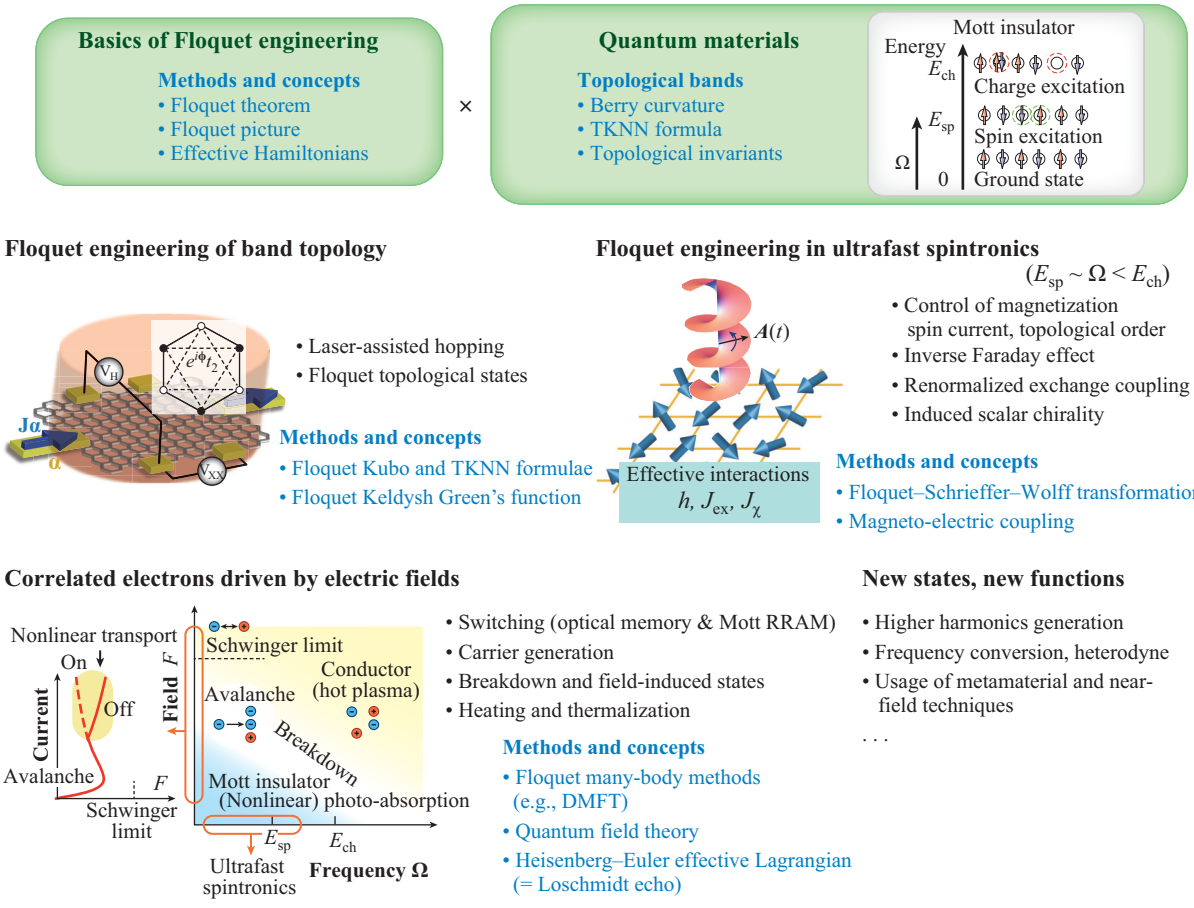

Figure 1

Floquet engineering in quantum materials. Various processes take place when an intense laser or electric field is applied to quantum materials with exotic properties such as topological bands (51, 52), Dirac and Weyl semimetals (53–55), and strong correlation (56). The keywords in blue denote methods and concepts useful to describe them. Abbreviations: DMFT, dynamical mean field theory; RRAM, resistivity random access memory; TKNN, Thouless–Kohmoto–Nitingale–den Nijs.

for the Hamiltonian and the Floquet state. With this representation, the time-dependent Schrödinger equation is mapped to an eigenvalue problem (17, 19),

$$\sum_m (H_{n-m} - m\Omega\delta_{mn})\,|\Phi_\alpha^m\rangle = \varepsilon_\alpha |\Phi_\alpha^n\rangle, \qquad 4.$$

in an extended Hilbert space. The index α labels eigenstates, and m and n are the Fourier mode indices. Now, the Hilbert space has been infinitely expanded, but this is compensated by the indefiniteness of ε.

One can view the index m as a position in the Floquet direction: The system described by Equation 4 is equivalent to a time-independent layered one-body system in which m labels the layers (**Figure 2**). The intralayer hopping is described by H_0, whereas $H_m (m \neq 0)$ give interlayer couplings. In addition, there is a static electric field in the Floquet direction coming from the

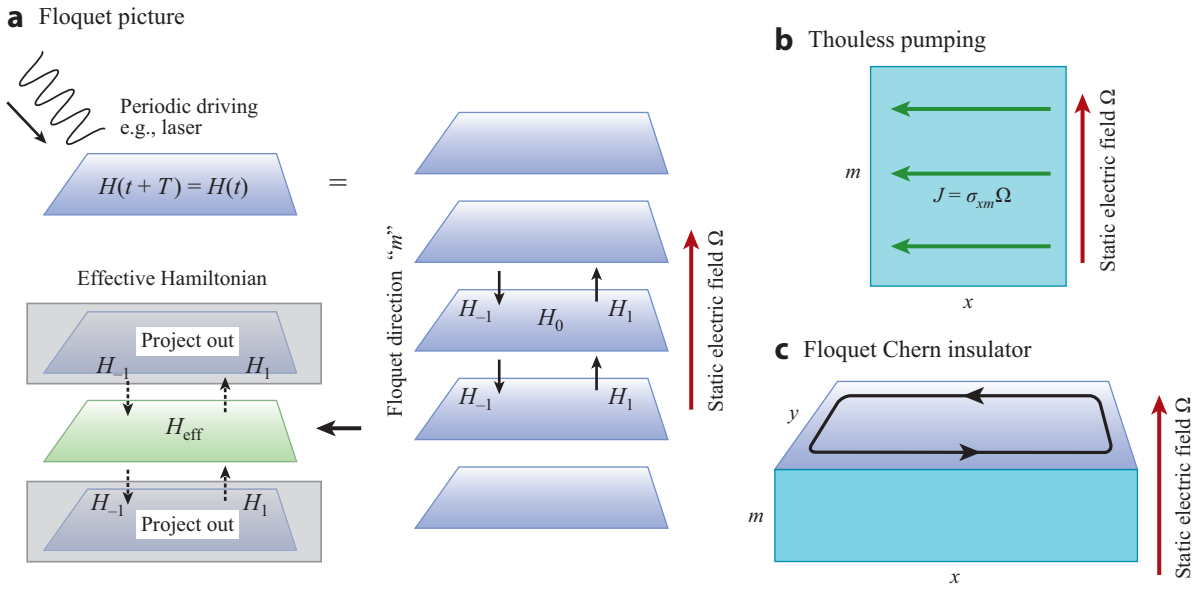

Figure 2

Floquet picture for one-body physics: (*a*) A mapping to a static higher-dimensional model gives an intuitive understanding of (*b*) Thouless pumping (Section 2.1) and (*c*) Floquet Chern insulators (Section 3). The effective Hamiltonian describes physics projected onto the original Hilbert space (Section 2.4).

$m\Omega$-term in Equation 4. This fictitious electric field Ω plays an important role in understanding the physics of driven systems. For small Ω, we have a lattice problem in higher dimensions in a weak electric field. If this model is a two-dimensional Chern insulator with a Hall coefficient σ_{xm}, a dissipationless current $j_x = \sigma_{xm}\Omega$ is generated, which is nothing but the Thouless pumping (57). For larger Ω, the layers become isolated energetically, and the state exhibits Wannier–Stark localization (along the Floquet direction). In such a situation, the high-frequency expansion is a powerful tool in understanding the physics systematically.

2.1. Thouless Pumping in the Floquet Picture

Thouless pumping (57) is probably one of the most well-known phenomenon in time-periodic systems. The Rice–Mele model (58), defined by

$$H(t) = -\sum_j [J + \delta_1 \cos \Omega t (-1)^j](c_{j+1}^\dagger c_j + \text{h.c.}) + \delta_2 \sin \Omega t \sum_j (-1)^j c_j^\dagger c_j, \qquad 5.$$

is a minimum model that shows charge pumping (J, static hopping; $\delta_{1,2}$, modulation parameter of the hopping and on-site potential). By interpreting Ωt as momentum in the Floquet direction, this model can be mapped to a two-dimensional lattice system (**Figure 3**) governed by the eigenvalue problem (Equation 4), with $H_0 = -J\sum_j (c_{j+1}^\dagger c_j + \text{h.c.})$ and $H_{\pm 1} = (1/2)\sum_j (-1)^j [-\delta_1 (c_{j+1}^\dagger c_j + \text{h.c.}) \pm i\delta_2 c_j^\dagger c_j]$. With this description, the Thouless pumping is nothing but the two-dimensional quantum Hall effect in the m-x plane (59). The Hall conductivity of this

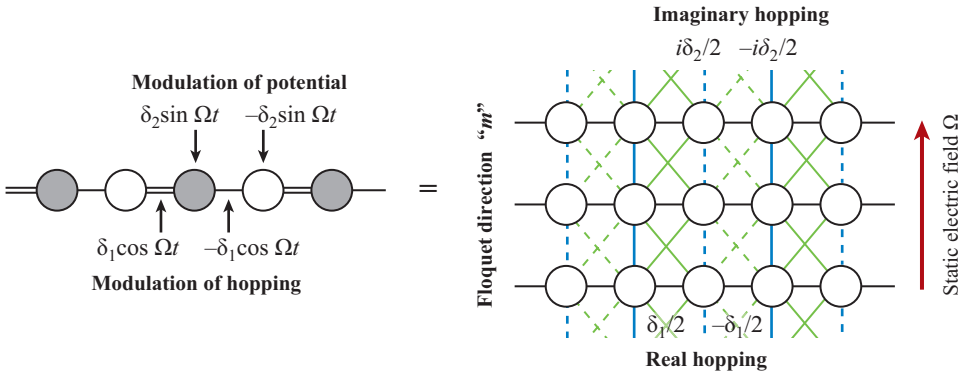

Figure 3

Floquet picture for Thouless pumping in the Rice–Mele model.

effective m-x plane is given by

$$\sigma_{xm} = i \sum_{\lambda} f_{\lambda} \int_0^T \frac{\mathrm{d}t}{2\pi} \int \frac{\mathrm{d}k}{2\pi} \left[\left\langle \frac{\partial \psi_{\lambda}}{\partial t} \middle| \frac{\partial \psi_{\lambda}}{\partial k} \right\rangle - \left\langle \frac{\partial \psi_{\lambda}}{\partial k} \middle| \frac{\partial \psi_{\lambda}}{\partial t} \right\rangle \right], \qquad 6.$$

which is nothing but the original expression derived by Thouless (57) and is equivalent to the TKNN (Thouless–Kohmoto–Nitingale–den Nijs) formula (60) with the y coordinate replaced by m. It becomes quantized ($\sigma_{xm} = \frac{2\pi}{h} m$, where $m = 0, \pm 1, \pm 2, \ldots$) as long as the gap does not close and the distribution f_{λ} is a constant within the band; i.e., the field strength Ω is smaller than the Landau–Zener tunneling threshold. In such situations, the relation $J = \sigma_{xm}\Omega$ states that an integer number of charge is transferred per unit time $T = 2\pi/\Omega$.

2.2. High-Frequency Expansion

Let us consider a situation in which the driving frequency Ω is much larger than other typical energy scales in the Hamiltonian so that the layers are isolated energetically. In this situation the eigenvalue problem of Equation 4 can be solved efficiently by performing (van Vleck's) degenerate perturbation theory starting from the unperturbed Hamiltonian with only the $m\Omega$-term (61, 62). After performing the perturbative expansion, the eigenvalue problem becomes decoupled in the Floquet direction. This means that the quasi-energy can be obtained as eigenvalues of the static Hamiltonian. This effective Hamiltonian has a universal form for time-periodic Hamiltonians (including many-body systems),

$$H_{\mathrm{eff}}^{\mathrm{vV}} = H_0 + \sum_{m \neq 0} \left(\frac{[H_{-m}, H_m]}{2m\Omega} + \frac{[[H_{-m}, H_0], H_m]}{2m^2\Omega^2} + \sum_{n \neq 0, m} \frac{[[H_{-m}, H_{m-n}], H_n]}{3mn\Omega^2} \right) + \mathcal{O}(\Omega^{-3}). \qquad 7.$$

For later convenience, we provide the effective Hamiltonian for free fermions described by $H(t) = \sum_{ij} J_{ij}(t) c_i^{\dagger} c_j$ with $J_{ij}(t+T) = J_{ij}(t) = \sum_m J_{ij}^m e^{-im\Omega t}$. The effective Hamiltonian is calculated to be (30)

$$H_{\mathrm{eff}}^{\mathrm{vV}} = \sum_{ij} \left[J_{ij}^{(0)} + J_{ij}^{(1)} + J_{ij}^{(2)} \right] c_i^{\dagger} c_j + \mathcal{O}(\Omega^{-3}), \qquad 8.$$

where the effective hopping is given as

$$J^{(0)}_{ij} = J^{0}_{ij}, \quad J^{(1)}_{ij} = \sum_{m\neq 0}\sum_{k} \frac{J^{-m}_{ik} J^{m}_{kj}}{m\Omega},$$

$$J^{(2)}_{ij} = \sum_{m\neq 0}\sum_{kl} \left(\sum_{n\neq 0} \frac{J^{-m}_{ik} J^{m-n}_{kl} J^{n}_{lj}}{mn\Omega^2} - \frac{J^{0}_{ik} J^{-m}_{kl} J^{m}_{lj} + J^{-m}_{ik} J^{m}_{kl} J^{0}_{lj}}{2m^2\Omega^2} \right). \quad 9.$$

2.3. Application to Many-Body Systems

When we consider many-body systems driven periodically, we must be careful because the system may heat up. In closed periodically driven systems, a state evolves as $|\psi(t)\rangle = \sum_\alpha c_\alpha e^{-i\varepsilon_\alpha t}|\Phi_\alpha(t)\rangle$, where $c_\alpha = \langle\Phi_\alpha(t_0)|\psi_0\rangle$ and $|\psi_0\rangle$ is the initial state at time $t_0 = 0$. $|\Phi_\alpha(t)\rangle$ are the Floquet states with quasi-energy ε_α. On stroboscopic time steps ($t = mT$), the solution $|\psi(t)\rangle$ has an identical form to that of the time evolution in static systems with the quasi-energy ε_α playing the role of the (usual) energy and $|\Phi_\alpha(t_0)\rangle$ the usual eigenstate.

In static nonintegrable many-body systems, for typical initial states, thermalization is expected to occur after a sufficiently long time evolution (63, 64). This implies that the periodically driven systems are also expected to thermalize because $\langle\psi(t)|\hat{O}|\psi(t)\rangle|_{t\to\infty} = \sum_\alpha e^{-\beta\varepsilon_\alpha}\langle\Phi_\alpha(t_0)|\hat{O}|\Phi_\alpha(t_0)\rangle$ should hold for an observable $\hat{O}$ in the stroboscopic time evolution. However, remember that ε_α was only defined modulo Ω, and such indefiniteness should not appear in physical quantities. The solution to this paradox was given in References 40 and 41, showing that $\langle\Phi_\alpha(t_0)|\hat{O}|\Phi_\alpha(t_0)\rangle$ is independent of α. In other words, all many-body Floquet states that we obtain by solving Equation 4 are featureless. This can be stated more intuitively by noting that in closed systems, many-body states that are constantly driven by an external periodic force keep on heating until the temperature goes to infinity.

Nevertheless, Floquet theory is still a useful framework in many-body systems. Heating should occur over a relatively long timescale for appropriately chosen driving so that there can be a nontrivial metastable state on a shorter timescale. By using an appropriate perturbative expansion and truncating out the slow heating processes coming from higher-order terms, we can describe this metastable state as an eigenstate of the effective Hamiltonian (43–45). In this situation, a periodically driven system will first "equilibrate" with the truncated Hamiltonian and eventually thermalizes to the true long time limit, i.e., the infinite temperature state. The first equilibration is termed the Floquet prethermalization, being a special case of prethermalization (65) known in quench dynamics (66, 67) (reviewed in References 68 and 69).

Electrons in solid states are subject to various open-system relaxation processes such as phonon scattering or coupling to an electron bath (substrate). When the pump is longer than their characteristic coupling time, the system converges to a nonequilibrium steady state, and the heating is balanced with the relaxation (34, 35). The nontrivial steady states of such systems can be studied by the Floquet Green's function method combined with an appropriate many-body technique such as nonequilibrium dynamical mean-field theory (9, 25). In Section 5, we try to sort out results in ultrafast and nonlinear experiments in correlated electron systems from the point of view of many-body Floquet dynamics.

2.4. Effective Hamiltonians

Although we have already introduced the concept of the effective Hamiltonian in Section 2.2, here we discuss its general aspect in more detail. We have obtained the form of the effective

static Hamiltonian (Equation 7) by the block-diagonalization of Equation 4 recast as regarding the interlayer transitions as virtual processes. If we consider this in the time domain, the construction of the effective Hamiltonian can be recast as a search for an appropriate time-periodic unitary transformation

$$\tilde{H} = U^{\dagger}(t)H(t)U(t) - iU^{\dagger}(t)\frac{\partial}{\partial t}U(t) \qquad 10.$$

that makes $\tilde{H}$ time independent. Although the existence of the transformation is assured by the Floquet theorem, such a transformation is not unique. One arbitrariness comes from the time-independent unitary transformation, by which we can generate new effective Hamiltonians once we obtain one static Hamiltonian. There is also an arbitrariness due to the indefiniteness of the quasi-energy.

One conventional effective Hamiltonian is the Floquet–Magnus (FM) Hamiltonian (70, 71), which can be obtained from the time-evolution operator over a period T as

$$H_{\mathrm{eff}}^{\mathrm{FM}} = \frac{i}{T}\ln\hat{T}\exp\left[-i\int_{t_0}^{t_0+T}H(s)\,\mathrm{d}s\right], \qquad 11.$$

where $\hat{T}$ denotes time ordering. Although the form of the Hamiltonian changes depending on the initial time t_0, those with different t_0 are related by unitary transformations. The van Vleck Hamiltonian (Equation 7) is also unitary equivalent to the FM Hamiltonian up to the truncation error.

The effective Hamiltonian depends on the perturbation schemes: An approximation more efficient than the high-frequency expansion can be constructed if we use the eigenbasis of $H_0 - m\Omega$, the intralayer term[1] in the Floquet picture (**Figure 2**), as the starting point of perturbation. Note that the high-frequency expansion (Equation 7) is using $m\Omega$ as the unperturbed Hamiltonian. For example, if a perturbation to H_0 is given by $V(t) = ve^{i\Omega t} + v^{\dagger}e^{-i\Omega t}$, the second-order contribution yields

$$\langle a|\delta H_{\mathrm{eff}}^{\mathrm{2nd}}|b\rangle = -\sum_{c}\left(\frac{\langle a|v|c\rangle\langle c|v^{\dagger}|b\rangle}{\Delta_{cb}-\Omega} + \frac{\langle a|v^{\dagger}|c\rangle\langle c|v|b\rangle}{\Delta_{cb}+\Omega}\right), \qquad 12.$$

where $H_0|a\rangle = E_a|a\rangle$ and $\Delta_{ab} = E_a - E_b$. This form is employed, e.g., in the theory of inverse Faraday effect (72). Application of this expansion (Equation 12) requires all the eigenstates of H_0, which are often difficult to obtain. We can still use a solvable part within the Hamiltonian to construct the basis and perform an expansion around it. For example, the Floquet–Schrieffer–Wolff transformation (strong coupling expansion) for the Hubbard model (73–76) expands as series of $1/(n_{\mathrm{D}}U - m\Omega)$ (where n_{D} is the doublon number), and the atomic Hamiltonian $U\sum_i n_{i\uparrow}n_{i\downarrow} - m\Omega$ is used to define the basis (to be explained in Section 4).

Among the variety of the effective Hamiltonians, we should adopt an appropriate one in accordance with a problem of interest. The FM Hamiltonian is directly related to the time evolution and suitable for the initial-value problem and quench dynamics. Because the FM Hamiltonian often does not respect the symmetry of the system, it is better to use the van Vleck expansion when we are interested in the properties of the Hamiltonian itself.

[1]There are also more general choices with nonblock-diagonal Hamiltonians (not decoupled in the Floquet direction), which are treated in the same way after a block diagonalization of the unperturbed Hamiltonian.

3. FLOQUET ENGINEERING OF BAND TOPOLOGY

In this section, as a representative example of Floquet engineering, we discuss properties of graphene irradiated by a circularly polarized laser (77). In particular, we focus on transport and response properties, and we introduce theoretical tools to relate the nontrivial Floquet states and response functions.

3.1. Laser-Irradiated Graphene

In graphene (53), carbon atoms form a honeycomb lattice whose low-energy effective model is described by a tight-binding model of the p_z orbital $H = -\sum_{ij}^{\mathrm{NN}} J_{ij} c_i^\dagger c_j$. Here, we take the sum over nearest-neighbor (NN) sites, and $J_{ij} = J$ is the hopping amplitude. The energy dispersion of this model has two inequivalent Dirac cones in the Brillouin zone, at K and K′ [$\boldsymbol{k} = (\pm 4\pi/3\sqrt{3}, 0)$]. The honeycomb tight-binding model in the circularly polarized laser is a prototype of the Floquet topological insulator (77–80). Let us see this by first employing the high-frequency expansion (Section 2.2). We introduce the laser electric field $\boldsymbol{E}(t) = -\partial_t \boldsymbol{A}(t)$ using the Peierls substitution as

$$J_{ij}(t) = J_{ij} \exp\left[-i \int_{\boldsymbol{R}_j}^{\boldsymbol{R}_i} \boldsymbol{A}(t) \cdot \mathrm{d}\boldsymbol{r}\right], \tag{13.}$$

where $\boldsymbol{R}_i$ is the position of site i, and the vector potential representing a circularly polarized laser is given as $\boldsymbol{A}(t) = (A\cos\Omega t, A\sin\Omega t)$. Then the Fourier components of the hopping amplitude are given as $J_{ij}^m = J\mathcal{J}_m(A)e^{im\phi_{ij}}$ with the bond angle $\phi_{ij} = -\tan^{-1}(R_i^x - R_j^x)/(R_i^y - R_j^y)$ and $\mathcal{J}_m$ being the m-th Bessel function of the first kind. The Fourier expansion of the hopping represents laser-assisted processes, absorbing or emitting m photons. We can then use Equation 9 to obtain an effective Hamiltonian

$$H_{\mathrm{eff}} = -\sum_{ij}^{\mathrm{NN}} J_{\mathrm{eff}} c_i^\dagger c_j + \sum_{ij}^{\mathrm{NNN}} iK_{\mathrm{eff}}\, \tau_{ij} c_i^\dagger c_j + J\mathcal{O}\left(\frac{J^2}{\Omega^2}\right), \tag{14.}$$

where τ_{ij} in the next-nearest-neighbor (NNN) term takes $+1$ (-1) for the hopping with a clockwise (counterclockwise) path (from j to i) on each hexagon. The effective hopping amplitudes are

$$J_{\mathrm{eff}} = J\mathcal{J}_0(A) \text{ and } iK_{\mathrm{eff}} = -i\frac{2J^2}{\Omega}\sum_{n=1}^{\infty}\frac{\mathcal{J}_n^2(A)}{n}\sin\frac{2\pi n}{3}. \tag{15.}$$

J_{eff} is obtained as a time average of the original Hamiltonian, where a reduction of the tunneling amplitude, known as the dynamic localization, occurs due to a renormalization factor $\mathcal{J}_0(A)$ (18). It is experimentally claimed in solids that this effect is realized (81). The effective NNN hopping iK_{eff} emerges from the two-step laser-assisted hopping process (see **Figure 4*a***). Equation 15 is nothing but the Hamiltonian of the Haldane model (82), and at the Dirac cones K and K′ the model exhibits a topological gap opening leading to a nontrivial Chern number. Chiral edge modes emerge in the quasi-energy spectrum (**Figure 4*b*,*c***), and their direction as well as the sign of the Chern number depends on the sign of K_{eff} that can be flipped by changing the polarization $\Omega \to -\Omega$.

Although the high-frequency expansion gives an intuitive picture for the Floquet topological phase transition, let us comment on the role played by the geometric phase in the gap opening. Through the Peierls substitution (Equation 13), a state with momentum $\boldsymbol{k}$ starts to move as $\boldsymbol{k} + \boldsymbol{A}(t)$ in momentum space. For a circularly polarized laser, this motion is circular (**Figure 5*a***), and the state acquires the Aharonov–Anandan phase (83) (or the nonadiabatic extension of the Berry

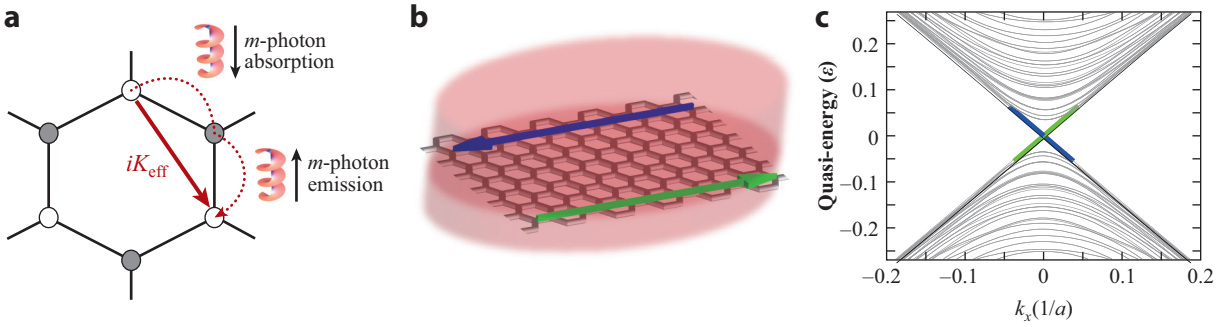

Figure 4

(*a*) Laser-assisted hopping (*dotted lines*) for the honeycomb lattice driven by a circularly polarized laser leads to an effective next-nearest hopping with a phase factor (Equation 14). Haldane's Chern insulator model (82) is obtained up to first order in the high-frequency expansion. (*b*) Chiral edge modes are induced under irradiation and this is seen in the (*c*) Floquet quasi-energy spectrum (78).

phase; 84) during the time evolution. The Floquet quasi-energy is written as

$$\varepsilon_\alpha = \langle\langle \Phi_\alpha | H(t) | \Phi_\alpha \rangle\rangle + \Omega \gamma_\alpha^{\mathrm{AA}}/2\pi, \qquad 16.$$

a sum of the dynamical phase and the Aharonov–Anandan phase. We have used the time-averaged inner product and matrix element of a time-dependent operator as $\langle\langle \Phi_\alpha | \Phi_\beta \rangle\rangle \equiv \frac{1}{T}\int_0^T \mathrm{d}t \langle \Phi_\alpha(t) | \Phi_\beta(t) \rangle = \sum_m \langle \Phi_\alpha^m | \Phi_\beta^m \rangle$ and $\langle\langle \Phi_\alpha | \mathcal{O} | \Phi_\beta \rangle\rangle = \frac{1}{T}\int_0^T \mathrm{d}t \langle \Phi_\alpha(t) | \mathcal{O}(t) | \Phi_\beta(t) \rangle$, respectively. At the Dirac points K and K′ [$\boldsymbol{k} = (\pm 4\pi/3\sqrt{3}, 0)$] (with a linearized dispersion), the Aharonov–Anandan phase becomes (77)

$$\gamma_\alpha^{\mathrm{AA}} \equiv T \langle\langle \Phi_\alpha | i\partial_t | \Phi_\alpha \rangle\rangle = \pm\pi \left\{ [4(A/\Omega)^2 + 1]^{-1/2} - 1 \right\}. \qquad 17.$$

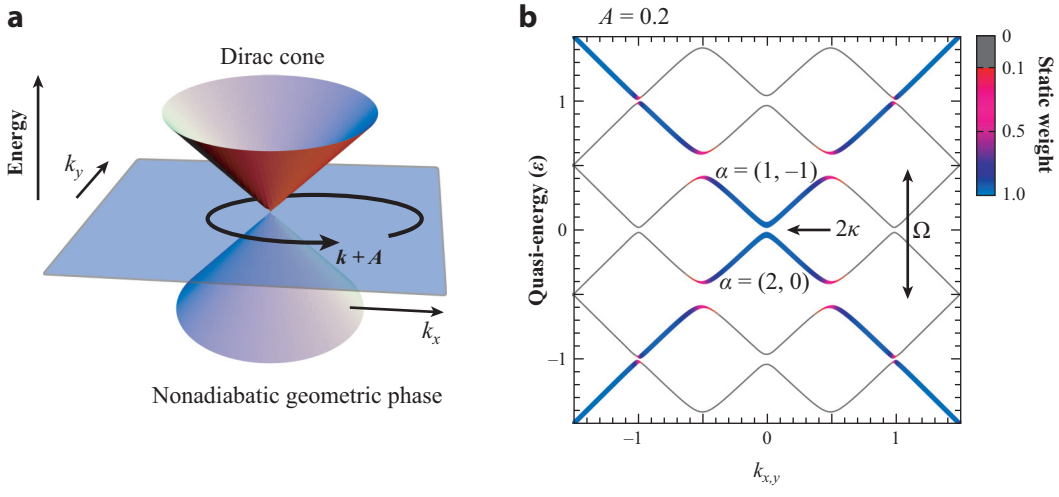

Figure 5

(*a*) States with momentum $\boldsymbol{k}$ acquire a geometric phase near the Dirac node. (*b*) The Floquet spectrum of a two-dimensional Dirac system in a circularly polarized laser. Color coding represents the static weight. Adapted from Reference 77.

In the adiabatic limit ($\Omega \to 0$), it converges to the Berry phase $\mp\pi$. The size of the gap 2κ can be evaluated as

$$2\kappa = \sqrt{4A^2 + \Omega^2} - \Omega. \tag{18.}$$

In artificial matter, periodically driven graphene was simulated in cold atoms in optical lattices (85) as well as in photonic wave guides (86), realizing the Haldane model (Floquet Chern insulator). In the solid states, a surface state of a topological insulator, which also hosts a two-dimensional Dirac node, was used to study the effect of a circularly polarized laser (87). The gapping of the Dirac node as well as the formation of replica bands as in **Figure 5*b*** was nicely demonstrated in a time-resolved ARPES experiment.

3.2. Floquet–Kubo and Floquet–Thouless–Kohmoto–Nitingale–den Nijs Formulae

In equilibrium, the quantum Hall effect at zero temperature is related to the Chern number through the TKNN formula. In a similar way, we need the Floquet–Kubo formula (88) and the Floquet–TKNN formula (77) to characterize the response of Floquet topological states. Here, we discuss nonlinear optical and transport properties in the presence of irradiation. When a strong laser ($A_{\rm ac}$) is applied to a system, the response to an additional weak perturbation can be changed. The response function is defined by a linear relation

$$j_i(\omega) = \sigma_{ij}(A_{\rm ac}; \omega) E_j(\omega) \tag{19.}$$

between the weak probe electric field E_j and the induced current j_i. The effect of the external AC field is taken into account using Floquet states as the basis. The optical response function for irradiated systems in the DC limit ($\omega \to 0$) becomes

$$\sigma_{ij}(\boldsymbol{A}_{\rm ac}) = i \int \frac{{\rm d}\boldsymbol{k}}{(2\pi)^d} \sum_{\alpha \in BZ_1} \sum_{\beta \neq \alpha} \frac{f_\beta(\boldsymbol{k}) - f_\alpha(\boldsymbol{k})}{\varepsilon_\beta(\boldsymbol{k}) - \varepsilon_\alpha(\boldsymbol{k})} \frac{\langle\langle \Phi_\alpha(\boldsymbol{k}) | J_j | \Phi_\beta(\boldsymbol{k}) \rangle\rangle \langle\langle \Phi_\beta(\boldsymbol{k}) | J_i | \Phi_\alpha(\boldsymbol{k}) \rangle\rangle}{\varepsilon_\beta(\boldsymbol{k}) - \varepsilon_\alpha(\boldsymbol{k}) + i0^+}, \tag{20.}$$

which was given in References 77, 78, and 89. Here, ε_α is the quasi-energy of Floquet state α, and f_α is its occupation fraction. Note that the index α is limited to the first Brillouin zone ($\varepsilon_\alpha \in [-\Omega/2, \Omega/2)$), whereas β is taken over the whole Floquet spectrum, which is extended from the original spectrum by the inclusion of photon-dressed replica states. The Hall coefficient is given by the Floquet–TKNN formula (77),

$$\sigma_{xy}(\boldsymbol{A}_{\rm ac}) = e^2 \int \frac{{\rm d}\boldsymbol{k}}{(2\pi)^2} \sum_{\alpha \in BZ_1} f_\alpha(\boldsymbol{k}) \left[\nabla_{\boldsymbol{k}} \times \boldsymbol{\mathcal{A}}_\alpha(\boldsymbol{k})\right]_z. \tag{21.}$$

The artificial gauge field and its associated Berry curvature is defined by

$$\boldsymbol{\mathcal{A}}_\alpha(\boldsymbol{A}_{\rm ac}; \boldsymbol{k}) = -i \langle\langle \Phi_\alpha(\boldsymbol{k}) | \nabla_{\boldsymbol{k}} | \Phi_\alpha(\boldsymbol{k}) \rangle\rangle, \quad \mathcal{B}_\alpha(\boldsymbol{A}_{\rm ac}; \boldsymbol{k}) = \nabla_{\boldsymbol{k}} \times \boldsymbol{\mathcal{A}}_\alpha(\boldsymbol{k}). \tag{22.}$$

Figure 6*a* shows the Berry curvature of a Floquet band, where we can see that peaks appear at the Dirac points. There are also concentric patterns around the Dirac points in which resonant hybridization occurs between the bands. There are two promising detection schemes for the Hall effect, which are the transport measurement in the presence of irradiation (**Figure 6*b*,*c***), and the

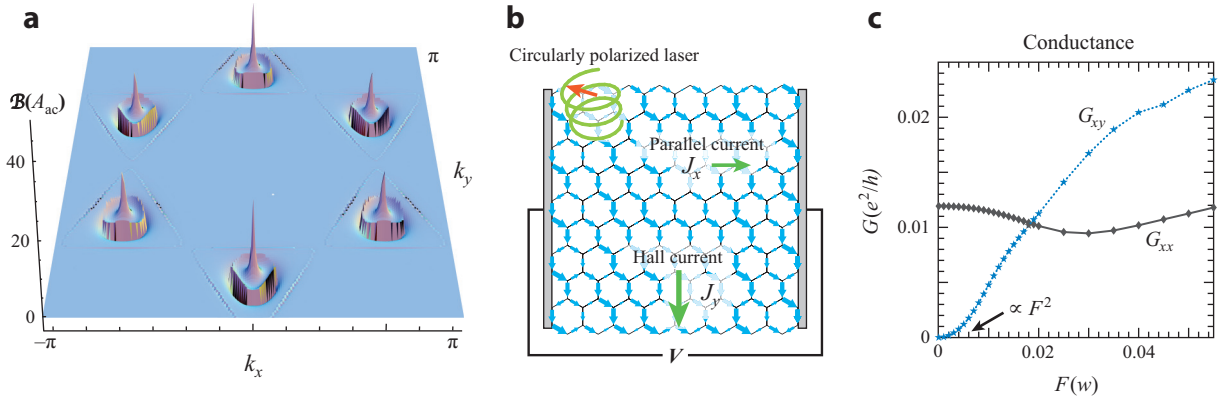

Figure 6

(*a*) Berry curvature of the Floquet band in graphene irradiated by a circularly polarized laser. Detection of Floquet Chern insulator can be done with (*b*) transport measurements of the (*c*) Hall conductance G_{xy} ($F = \Omega A_{ac}$) (77). Adapted from Reference 77.

time-resolved Kerr effect (89, 90). In the Kerr effect, the polarization angle of a probe laser is shifted by (91)

$$\Theta_H \sim \left(\sigma_{xy} \text{ in units of } \frac{e^2}{h}\right) \times 6.3 \text{ mrad} \qquad 23.$$

when it passes through a quantum Hall state. The Hall conductivity is not necessarily quantized in a Floquet Chern insulator because the electrons are photoexcited and the distribution function f_α is not the simple zero-temperature Fermi distribution. However, there have been several numerical analyses finding conditions for a quantized Hall coefficient in open systems (89, 92).

4. FLOQUET ENGINEERING IN ULTRAFAST SPINTRONICS

Spintronics is a new branch of electronics in which the spin degrees of freedom are used to carry and store information via spin currents and magnetization (93). In ultrafast spintronics, a laser is used to control spins and magnetism on the timescales of picoseconds or faster (6, 94, 95). A direct way to access spins is by the Zeeman coupling that couples to the magnetic field component of laser. Another relevant coupling is the magnetoelectric (ME) coupling that allows the electric field to interact with the polarization that depends on the spins. Several types of ME couplings are proposed (reviewed in Reference 96) such as (*a*) inverse Dzyaloshinskii–Moriya (DM) model (97, 98) $\boldsymbol{P} \propto \boldsymbol{e}_{\boldsymbol{r},\boldsymbol{r}'} \times (\boldsymbol{S}_{\boldsymbol{r}} \times \boldsymbol{S}_{\boldsymbol{r}'})$ and (*b*) exchange striction model $\boldsymbol{P} \propto \boldsymbol{\pi}_{\boldsymbol{r},\boldsymbol{r}'} \times (\boldsymbol{S}_{\boldsymbol{r}} \cdot \boldsymbol{S}_{\boldsymbol{r}'})$.

The ideas of Floquet engineering and effective Hamiltonians can be applied to ultrafast spintronics. Because the spin degrees of freedom originate from electrons, the construction of the effective Hamiltonian has different levels of approximation illustrated in **Figure 7**.

1. Electronic model: If direct electronic excitations are involved, we should start the construction from an electronic model. A classic example is the inverse Faraday effect studied by Pershan et al. (72), in which they used Equation 12 to obtain an effective Zeeman coupling $\delta H_{\text{eff}} = b_{\text{eff}} S_z$ for electron systems in circularly polarized light applied along the z axis. The effective magnetic field, b_{eff}, obtained by considering virtual electronic excitations,

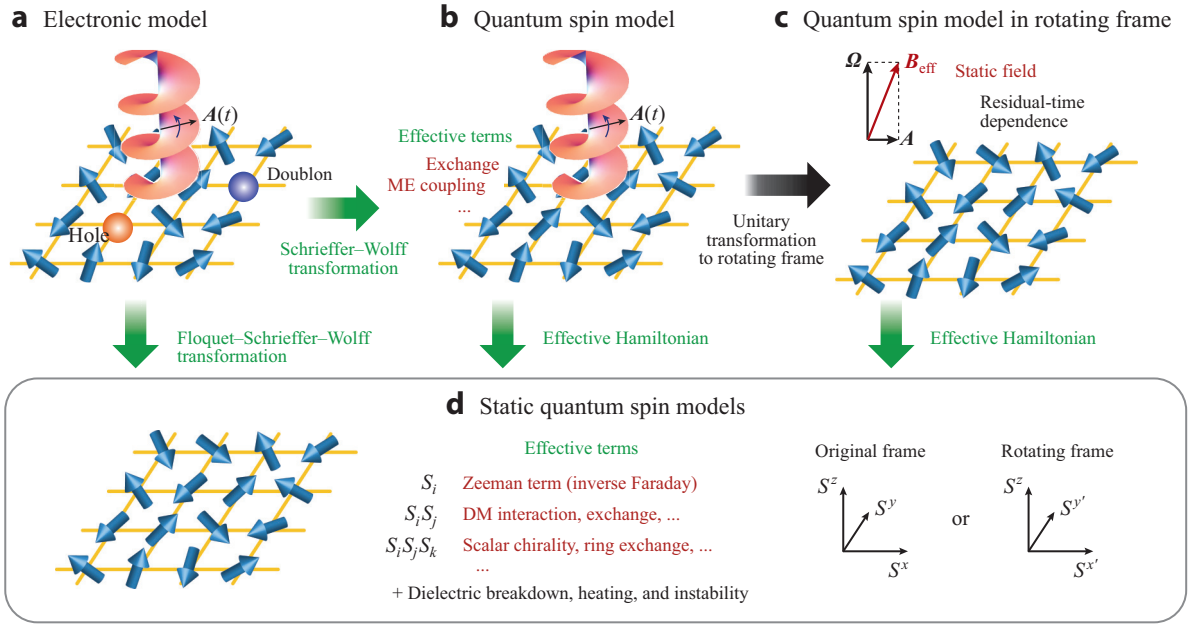

Figure 7

Effective theories for Floquet engineering in ultrafast spintronics: (*a*) The starting system is the electronic models, e.g., band ferromagnets and Mott insulators, under irradiation. (*b*) A time-dependent spin model is obtained by assuming that the field is weak and Ω much smaller than the charge gap. (*c*) For a circularly polarized laser, moving to the rotating frame gives a static magnetic field. (*d*) Effective Hamiltonians can be obtained by using appropriate expansion schemes. Abbreviation: DM, Dzyaloshinskii–Moriya.

is a nonlinear function of the laser strength and frequency and can be extremely large (6, 94, 95). However, in strongly correlated insulators such as the Mott insulator, using the second-order perturbation Equation 12 is difficult, and thus it is plausible to combine the Floquet picture with the standard Schrieffer–Wolff transformation (73–76), which is explained in Section 4.1.

2. Quantum spin model: Another way to construct the effective theory is to start from quantum spin models including the coupling to laser fields (99, 100); i.e.,

$$H(t) = H_0 - g\mu_B \boldsymbol{B}(t) \cdot \boldsymbol{S} - \boldsymbol{E}(t) \cdot \boldsymbol{P}. \quad 24.$$

Here, H_0 denotes the original quantum spin models, e.g., the Heisenberg model, and the other terms are the Zeeman and ME coupling. This approach is justified when the field is much slower than the electron dynamics ($\Omega \ll E_{ch}$). An effective Hamiltonian for circularly polarized laser irradiation based on the high-frequency expansion (Equation 7),

$$\delta\mathcal{H}_{eff} = -\frac{i}{2\Omega}\left\{\beta^2[S^x, S^y] + \alpha\beta([\tilde{P}^x, S^x] + [\tilde{P}^y, S^y]) + \alpha^2[\tilde{P}^x, \tilde{P}^y]\right\}, \quad 25.$$

$$\sim 1 \text{ spin term} + 2 \text{ spin term} + 3 \text{ spin term}, \quad 26.$$

can be obtained (100). Here, the dimensionless polarization is defined by $\tilde{\boldsymbol{P}} = \boldsymbol{P}/g_{me}$ with g_{me} being the ME coupling constant and $\alpha = g_{me}E_0$ and $\beta = g\mu_B E_0 c^{-1}$. Evaluating the commutators, we obtain terms that are products of 1, 2, and 3 spins, for example, the Zeeman, DM, and spin chirality, and their precise forms depend on the ME coupling reflecting the symmetry of the crystal.

3. Quantum spin model in the rotating frame: In the special case where the applied field is circularly polarized, we can obtain an exact form of the effective Hamiltonian without carrying out the perturbative expansion: A quantum spin system in a rotating magnetic field described by $H(t) = H_0 + A\cos(\Omega t)S_x + A\sin(\Omega t)S_y$ can be mapped to a simple static magnetization problem $\tilde{H} = H_0 + \Omega S_z + AS_x$ by moving to the rotating frame using a unitary transformation $U(t) = \exp(i\Omega S_z t)$, assuming that H_0 is rotationally symmetric around the z axis. The effective magnetic field $h_{\text{eff}} = (A, 0, \Omega)$ acting on the mapped system can be large, e.g., Ω in terahertz corresponds to a few teslas and can be used to orient the spins and induce magnetization (101, 102).

4.1. Floquet–Schrieffer–Wolff Transformation

Here, we see how the laser electric field influences the spin degree of freedom via the framework of the strong-coupling expansion for the periodically driven Hubbard model. We introduce the Hubbard model under a laser electric field,

$$H(t) = T(t) + UD = -\sum_{ij\sigma} t_{ij} e^{-iA_{ij}(t)} c^\dagger_{i\sigma} c_{j\sigma} + U\sum_i n_{i\uparrow} n_{i\downarrow}, \qquad 27.$$

where t_{ij} describes hopping of electrons c from site j to i, and U is the on-site density interaction. The oscillating electric field is described by the Peierls phase, $A_{ij}(t)$.

First, let us quickly review the strong-coupling expansion of the Hubbard model in the static case. In the strong coupling limit of the Hubbard model $t_{ij} = 0$, the ground states are any electron configurations with no double occupancy, which have a macroscopic degeneracy. In particular, the subspace spanned by the ground states at half filling is described by spin configurations. The macroscopic degeneracy lifts when we introduce the hopping $t_{ij} \neq 0$ as a perturbation. The low-energy effective model that describes this lift is the Heisenberg model, where the antiferromagnetic exchange interaction J_{ij} is given as $J_{ij} = 4t_{ij}^2/U$.

To perform a perturbative expansion of macroscopically degenerate systems in a systematic manner, it is convenient to employ the canonical transformation (Schrieffer–Wolff transformation). Namely, we consider a unitary transformation e^{iS} as a series in t_{ij} and determine it order by order to block-diagonalize the Hamiltonian with respect to double-occupancy D, which classifies the eigenstates in the atomic limit. We then obtain the effective spin Hamiltonian as the $D = 0$ sector of the transformed Hamiltonian. Our goal in this section is to see the influence of an external field on the Mott insulator described by this strong-coupling expansion.

One can extend this scheme to a time-dependent situation by considering a time-dependent transformation. We first perform a series expansion of the transformed Hamiltonian $H'(t)$ in $S(t)$ as (103, 104)

$$\begin{aligned} H'(t) &= e^{iS(t)}H(t)e^{-iS(t)} - e^{iS(t)}i\partial_t e^{-iS(t)} \\ &= H(t) + [iS(t), H(t) - i\partial_t] + \frac{1}{2}[iS(t), [iS(t), H(t) - i\partial_t]] + \cdots, \end{aligned} \qquad 28.$$

and further expand $S(t)$ in t_{ij} as $S(t) = S^{(1)}(t) + S^{(2)}(t) + \cdots$. Then the first-order term of $H'(t)$ is given as

$$H'^{(1)} = T(t) + [iS^{(1)}(t), UD] - \partial_t S^{(1)}(t). \qquad 29.$$

To block-diagonalize $H'(t)$, we determine S by solving a set of differential equations

$$\partial_t S^{(1)}_{+d}(t) = -idUS^{(1)}_{+d}(t) + T_{+d}(t) \tag{30.}$$

for $d \neq 0$, where S_{+d}, T_{+d} denote terms that increase double occupancy D by d. Although one can solve these for arbitrary fields with an appropriate boundary condition, here we consider a monochromatic laser $A_{ij}(t) = A_{ij}\cos(\Omega t - \phi_{ij})$ and consider a time-periodic solution. Using second-order perturbation, we obtain the Heisenberg model with a modified exchange interaction (73)

$$J_{ij}(t) = \sum_{m,n}(-1)^m \frac{4|t_{ij}|^2 \mathcal{J}_{n+m}(A_{ij})\mathcal{J}_{n-m}(A_{ij})}{U-(m+n)\Omega}\cos 2m(\Omega t - \phi_{ij}), \tag{31.}$$

where $\mathcal{J}_m$ is the m-th Bessel function. This is the lowest-order contribution of the electric field to the spin interaction. The obtained spin interaction is time periodic, and the effective static Hamiltonian can be obtained by performing a high-frequency expansion (Section 2.2).

Although we have considered a simple spin interaction in the Hubbard model here, there are various mechanisms to produce effective spin interactions via virtual processes, such as the Kugel–Khomskii coupling in multiband systems (105, 106), superexchange coupling in multiferroic systems (98), and anisotropic spin coupling under strong spin-orbit coupling (107, 108). For all of these, we can apply the above described scheme.

As we mentioned in Section 2.3, the heating processes due to higher-order perturbations are (implicitly) truncated out in the present scheme. Such processes associated with charge excitations emerge as a divergence of the expansion (due to a vanishing energy denominator $DU - m\Omega$). This divergence originally comes from an additional degeneracy between sectors with different D in the atomic limit.[2] Hence, we have to be aware that, in the true degenerate perturbation theory, one cannot block-diagonalize the Hamiltonian with D (nor m), and the above scheme is valid up to a certain finite order (75). The intersecting (changing D) terms are nothing but charge excitations, which lead to the heating. It is a general property of the effective Hamiltonian approach that the heating processes emerge as a divergence of the series expansion, and the error due to the truncation of the expansion gives a finite (but very long, in many cases) lifetime (43–45, 50).

4.1.1. Control and detection of spin chirality using laser. Although we have confirmed the modification of the exchange interaction, a more intriguing possibility is to induce an emergent interaction term that is absent in a static model by irradiating with a laser. This can be achieved by applying a field that breaks some symmetry of the original system. For instance, time-reversal symmetry is broken when circularly polarized laser irradiation is applied. If we continue the strong-coupling expansion to fourth order (**Figure 8*a***), the emergent term is the scalar spin chirality term $\chi_{ijk} = \boldsymbol{S}_i \cdot (\boldsymbol{S}_j \times \boldsymbol{S}_k)$. A classical spin configuration with a nonzero scalar chirality is shown in **Figure 8*b*** for illustration. Upon irradiation, an effective scalar chirality term $\delta H_{\rm eff} = \sum_{ijk} J_{\chi,ijk}\chi_{ijk}$ with

$$J_{\chi,ijk} = -4|t_{ij}|^2|t_{jk}|^2 \sum_{l,n}\sum_{m\neq 0}\left\{\frac{\mathcal{J}_{l+m}(A_{ij})\mathcal{J}_l(A_{ij})\mathcal{J}_{n+m}(A_{jk})\mathcal{J}_n(A_{jk})\sin m(\phi_{ij}-\phi_{jk})}{(U-l\Omega)(U-n\Omega)[U-(l+n+m)\Omega]}\right.$$
$$\left. + \frac{\mathcal{J}_{l+m}(A_{ij})\mathcal{J}_{l-m}(A_{ij})\mathcal{J}_{n+m}(A_{jk})\mathcal{J}_{n-m}(A_{jk})\sin 2m(\phi_{ij}-\phi_{jk})}{m\Omega[U-(l+m)\Omega][U-(n+m)\Omega]}\right\} \tag{32.}$$

[2]For example, when $U/\Omega = p/q$ with coprime p, q, the quasi-energy $\epsilon = DU - m\Omega$ is zero not only for $(D, m) = (0, 0)$ but also for $(q, p), (2q, 2p), \ldots$.

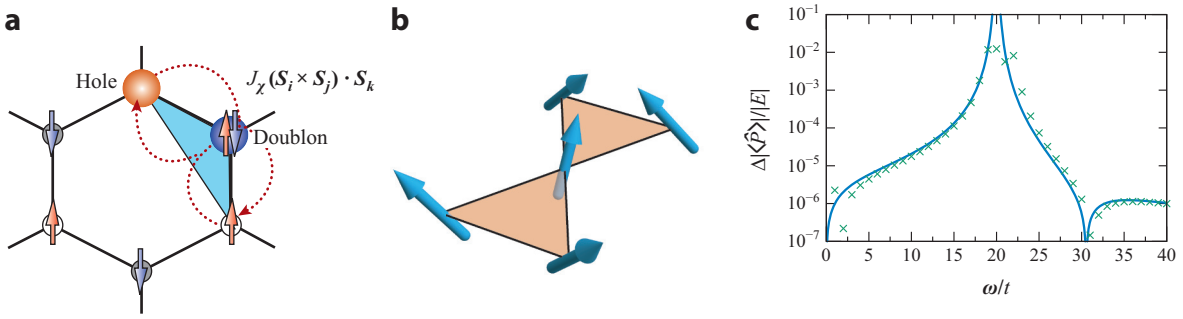

Figure 8

(*a*) Laser-assisted virtual hopping process leading to the scalar spin chirality term. (*b*) Classical configuration of spins with nonzero scalar chirality, $(\hat{\boldsymbol{S}}_i \times \hat{\boldsymbol{S}}_j) \cdot \hat{\boldsymbol{S}}_k$. (*c*) Circular dichroism: Difference of the induced electric polarization between left and right circularly polarized lasers, as a function of the photon energy. Crosses are numerical results for a three-site Hubbard cluster, and the solid curve is obtained from Equation 34.

emerges (75, 76). This opens the intriguing possibility of Floquet engineering exotic quantum phases such as a chiral spin liquid phase[3] (110).

The light-induced interaction also has a potential application as a new probe: For the above example, the circularly polarized laser acts as a conjugate field to the scalar spin chirality for general Mott insulators, in analogy with the magnetic field being conjugate to the spin. Namely, the coupling constant for the scalar chirality is reduced to

$$J_{\chi,ijk} \sim \frac{2\mathcal{A}_{ijk}|t_{ij}|^2|t_{jk}|^2\Omega(7U^2-3\Omega^2)}{U^2(U^2-\Omega^2)^3} i(\boldsymbol{E}^* \times \boldsymbol{E})_z, \qquad 33.$$

in the leading order of the field amplitude, where $\mathcal{A}_{ijk}$ is the area enclosed by sites i, j, k. The interaction term describes the modulation of the dielectric function proportional to the scalar chirality when it is viewed as a term in the Hamiltonian of the electromagnetic field. From Equation 33, the modulation is obtained as an imaginary off-diagonal part leading to circular dichroism (75)

$$\epsilon_{xy}(\omega) = i\sum_{ijk} \frac{4|t_{ij}|^2|t_{jk}|^2\omega(7U^2-3\omega^2)}{U^2(U^2-\omega^2)^3} \mathcal{A}_{ijk}\left\langle(\hat{\boldsymbol{S}}_i \times \hat{\boldsymbol{S}}_j)\cdot\hat{\boldsymbol{S}}_k\right\rangle. \qquad 34.$$

In other words, one can read out the presence of the scalar chirality via the circular dichroism. **Figure 8*c*** shows the difference of the dielectric function between circularly polarized light with a different chirality.

4.1.2. Validity of the expansion and candidate materials. The effective Hamiltonian approach is only valid on a timescale shorter than that of heating. In Mott insulators, creation of doublon–hole pairs makes the system conducting and destroys the spin picture. There are several sweet spots suitable for Floquet engineering in ultrafast spintronics. (*a*) High-frequency regime: When Ω exceeds both U and t, several doublon–hole pairs must be created simultaneously, which is a slower process. Heating becomes exponentially slow in this case (68). Candidate materials are organic Mott insulators (111) because their energy scale is an order of magnitude smaller than that of cuprates. (*b*) Subgap regime $\Omega < \Delta_{\text{Mott}}$: This is an attractive regime because many Mott

[3]Floquet chiral spin liquid with Majorana edge modes is proposed in Kitaev systems (109) under a circularly polarized laser (99). This theory starts from the driven quantum spin model.

insulators have gaps around and above 1 eV (56), and one can use mid-infrared lasers to access the spins.

When the field becomes stronger, charge excitations become nonnegligible due to higher-order processes such as multiphoton absorption, tunneling, and even electron avalanche. This is a problem for spintronics applications but opens a new possibility for a photoinduced phase transition, which we explain in the next section.

5. CORRELATED ELECTRONS DRIVEN BY ELECTRIC FIELDS

Ultrafast phenomena in strongly correlated electron systems driven by intense laser pulses have been studied during the past decades, starting from pioneering work in organic molecular compounds (112, 113) and vanadium oxides (114) that are associated with structural lattice dynamics (see **Figure 9**, ❶). In many cases, the structural change can be explained through the Franck–Condon picture (1). When electrons are excited, the lattice, feeling the Hellmann–Feynman force from the electrons, is deformed from the original structure (OFF) to a metastable excited state (ON). This switching can be used to realize an optical memory. In cuprates the concept of photodoping (**Figure 9**, ❷), i.e., creating doublon (electron)–hole pairs as transient carriers by laser irradiation, was introduced (115). Since then, the time resolution, intensity, and the flexibility to adjust the photon energy Ω of the pump laser have improved drastically (reviewed in References 1–5, 7, 9–12, and 13).

Let us explain the sequential processes that take place during and after the laser pulse with the general Floquet many-body physics, explained in Section 2.3, again in mind. First, we note that the physics strongly depends on the pulse duration, ranging from a few femtoseconds in the near-infrared regime ($\Omega \sim 1.5$ eV) to picoseconds (10^3 fs) for terahertz lasers (1 THz = 4.1 meV). The typical timescale of electron dynamics is femtoseconds, and thus for electrons irradiated by terahertz lasers the duration of the pulse is long enough that we expect to see the DC-field physics realized in transistor-like devices with applied bias voltage (14–16).

Using ultrashort pulses (**Figure 9*a***), it is now possible to observe quantum coherent dynamics in strongly correlated electron systems such as ultrafast switching and relaxation (**Figure 9**, ❸) toward a Mott insulator (116) or toward a metal (117), and it is even possible to see interference oscillations (**Figure 9**, ❹) between the Mott insulating groundstate and the excited state with a doublon–hole pair (118). Interestingly, almost at the same time, relaxation dynamics and doublon decay in a strongly interacting fermionic system were observed in cold atoms in optical traps, and this was realized by dynamically changing the trap (119). The dynamical control of lattice structure is also used in solid states, and this is done by exciting coherent phonon oscillations (**Figure 9**, ❺) to optimize the lattice structure with an aim of driving the electronics into interesting nonequilibrium phases such as a superconductor (13, 120–122).

In the DC limit (**Figure 9*b***) accessible by terahertz pump or nonlinear transport devices, the electrons are excited continuously and at the same time experience various relaxation processes, and their balance may realize interesting nonequilibrium steady states. The main relaxation mechanism is through emission of bosons, e.g., phonons, photons, and spin fluctuations. In DC devices made from strongly correlated materials, one goal is to realize a Mott RRAM (resistivity random access memory) (**Figure 9**, ❻), a device with an IV-characteristic showing switching behaviors (14–16, 123–125). This can be considered a DC limit of the optical switch. The electron avalanche (**Figure 9**, ❼) is an important excitation mechanism that exponentially increases the carrier density, leading to switching to a conducting state (126) (also demonstrated in a terahertz laser–excited semiconductor; Reference 127).

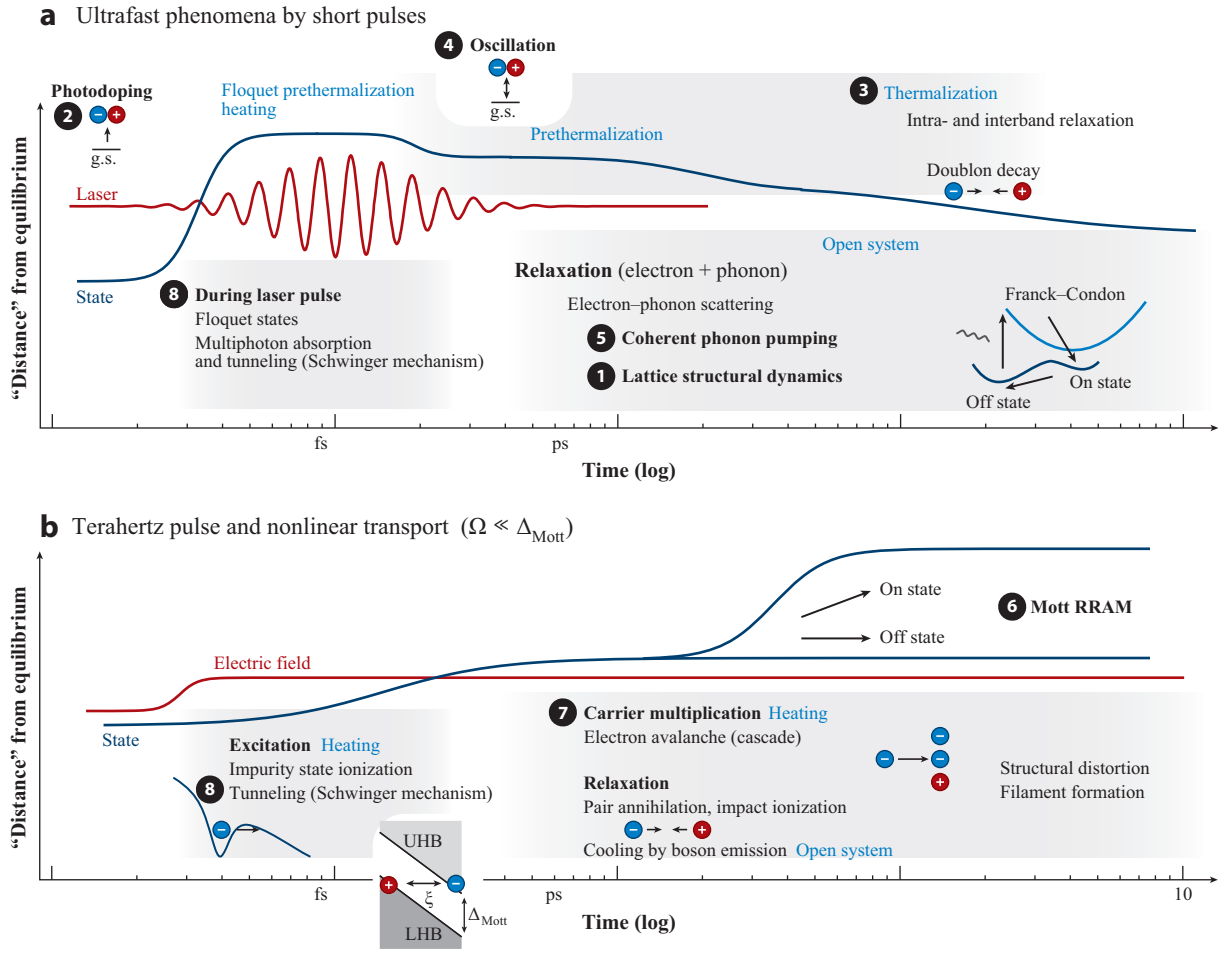

Figure 9

Processes taking place in pump-probe experiments with (*a*) ultrashort pulses and (*b*) longer pulses or nonlinear DC devices. The blue keywords roughly correspond to the many-body processes explained in Section 2.3. Abbreviations: fs, femtosecond; g.s., ground state; LHB, lower Hubbard band; ps, picosecond; RRAM, resistivity random access memory; UHB, upper Hubbard band.

It is still not easy to experimentally study the electron dynamics (**Figure 9**, ❽) during the pulse duration in strongly correlated materials because the typical pulse duration is a few to tens of femtoseconds. In contrast, theoretical studies using the driven Hubbard model (Equation 27) have been done extensively (24, 26, 128–134).

1. Laser-driven conducting state at resonance ($\Omega \sim \Delta_{\text{Mott}}$): In the presence of an AC electric field resonant with the Mott gap, the system evolves to a photoinduced metallic state within a short time. The doublon–hole pairs are resonantly created by the field and, at the same time, are destroyed through stimulated emission, so the system reaches a transient metastable state (26). In 1D, this state shares common features with the equilibrium Tomonaga–Luttinger liquid, such as spin charge separation. Such a metallic state can be captured by combining the Floquet method with the fermion–boson correspondence (26) or using the Floquet–Schrieffer–Wolff transformation (135).

2. Dielectric breakdown and the Keldysh crossover ($\Omega < \Delta_{\rm Mott}$) (128, 129, 134): Starting from the Mott insulating ground state, the application of subgap AC electric fields triggers dielectric breakdown through quantum tunneling or multiphoton absorption. The Loschmidt echo captures how a state $|\psi(t)\rangle = e^{-iHt}|\psi(0)\rangle$ is excited from the initial state and is defined by their overlap $\langle\psi(0)|e^{-iHt}|\psi(0)\rangle$. If the overlap decays as $\langle\psi(0)|e^{-iHt}|\psi(0)\rangle \sim e^{-i\mathcal{L}'t-\mathcal{L}''t}$ ($\mathcal{L}', \mathcal{L}''$: real), then $\Gamma = 2\mathcal{L}''$ characterizes the decay of the initial state, whereas $\mathcal{L}'$ is the Aharonov–Anandan phase (83). In quantum electrodynamics (QED) in an external field background, the Loschmidt echo was studied and defines the Heisenberg–Euler–Schwinger effective Lagrangian (136–139). This was adapted to (interacting) lattice models using the ground state–to–ground state amplitude (5, 129),

$$\mathcal{L}(F) = -\lim_{\tau\to\infty}\frac{i}{\tau V}\ln\langle 0|\hat{T}e^{-i\int_0^\tau F(s)\hat{X}(s)\,{\rm d}s}|0\rangle, \qquad 35.$$

where $F = A\Omega$ is the electric field, V the volume, and $\hat{X} = \sum_i i n_i$ is the position operator in the interaction representation $\hat{X}(t) = e^{itH_0}\hat{X}e^{-itH_0}$, where the original lattice Hamiltonian H_0, e.g., Hubbard Hamiltonian, is used. The real part of the effective Lagrangian is related to the field-induced electron polarization, $P(F) = \frac{\partial}{\partial F}{\rm Re}\mathcal{L}(F)$, and reduces to the Berry phase formula (140, 141) in the weak DC field limit. The imaginary part of the effective Lagrangian gives the decay rate, $\Gamma(F)/V = 2{\rm Im}\ \mathcal{L}(F)$, of the insulating ground state. The leading contribution to $\Gamma(F)/V$ comes from the doublon–hole creation, a process known in QED as the Schwinger effect (138, 139). For the 1D Hubbard model, one can use the Bethe ansatz of the non-Hermitian Hubbard model combined with the imaginary time method to evaluate the creation probability of doublon–hole pairs (132, 134),

$$\mathcal{P}_{\rm dh} \sim \begin{cases} \left(\frac{F_0\xi}{\hbar\Omega}\right)^{2\frac{\Delta_{\rm Mott}}{\Omega}} & \gamma \gg 1 \text{ (multiphoton)} \\ \exp\left[-\frac{\pi}{2}\frac{\Delta_{\rm Mott}}{\xi F_0}\left(1-\frac{\pi}{16}\gamma^2+\cdots\right)\right] & \gamma \ll 1 \text{ (tunneling)} \end{cases}, \qquad 36.$$

for AC fields $F(t) = F_0\cos\Omega t$. The correlation length ξ characterizes the size of the doublon–hole pairs existing in the ground state as a quantum fluctuation (142), and the Keldysh parameter that separates tunneling-dominant from multiphoton-dominant creation is defined by $\gamma = \frac{\Omega}{F_0\xi}$. Reaching and exceeding the Schwinger limit, $F_{\rm Sch} = \frac{\Delta_{\rm Mott}}{\xi}$, is a challenging problem, and typically this is impossible because the electron avalanche occurs below the limit (126, 143) (also known in QED; 144). Recently, the Schwinger limit was reached and exceeded in correlated insulators, and tunneling breakdown (Equation 36, *lower*) was experimentally verified (145, 146). These outstanding results were made possible by using a laser pulse that is short enough to suppress the heating and avalanche cascade effect.

6. OUTLOOK

One of the most fascinating aspects of Floquet engineering is that it is becoming a common language for researchers with diverse backgrounds in areas such as strongly correlated electron systems, artificial matter, and nonequilibrium statistical mechanics. High-energy physics and quantum field theory (136–139) are also great sources of ideas and motivations for condensed matter physicists, and the interaction between these two areas is expected to fertilize the field. In closing, let us mention some challenges that may be interesting for future developments.

1. Tailored fields from metamaterial plasmonics: To make Floquet-engineered devices fit inside our pockets, we need to replace the laser with a more efficient field generator, and the

usage of metamaterials and near-field optics will be an important step in this direction. Although they must be triggered by a pulse laser, metamaterials have demonstrated that electric fields exceeding 1 MV/cm (143) or magnetic fields of 1 Tesla (147), oscillating in the terahertz regime, can be generated. Interestingly, the fields are tailored by the structure and are different from the traveling electromagnetic field in the vacuum. It would be interesting to look for Floquet states that utilize this freedom.

2. Phase transition in a nonequilibrium state: Strongly motivated by recent experiments on light-induced superconductivity (13, 120–122), a variety of theoretical research studies have been done on driven correlated open systems (32, 36, 37, 148). The DC counterpart, i.e., phase transitions that occur in nonlinear devices (14–16, 29, 149), also show interesting properties (150) and provide challenges to theorists.
3. New devices from the new principle: It is interesting to look for functions of Floquet states that static systems cannot have. Devices that have an output signal with nontrivial frequencies due to the dynamics of the Floquet state have been proposed using correlated electrons (151, 152) and even single spins (153).

The future of this rapidly growing field holds a wealth of new possibilities, and we look forward to observing, and hopefully contributing to, its development in the coming years.

DISCLOSURE STATEMENT

The authors are not aware of any affiliations, memberships, funding, or financial holdings that might be perceived as affecting the objectivity of this review.

ACKNOWLEGMENTS

We gratefully acknowledge Naoto Tsuji, Takuya Kitagawa, Hideo Aoki, Shintaro Takayoshi, Masahiro Sato, Aditi Mitra, Hossein Dehghani, Takahiro Mikami, Eugene Demler, Liang Fu, André Eckardt, and Achilleas Lazarides for useful discussions, and financial support from the Max Planck Society.

LITERATURE CITED

1. Nasu K. 2004. *Photoinduced Phase Transitions*. Singapore: World Sci.
2. Iwai S, Okamoto H. 2006. *J. Phys. Soc. Jpn.* 75:011007
3. Koshihara S, Kuwata-Gonokami M. 2006. *J. Phys. Soc. Jpn.* 75:011001
4. Yonemitsu K, Nasu K. 2008. *Phys. Rep.* 465:1–60
5. Oka T, Aoki H. 2008. In *Quantum and Semi-classical Percolation and Breakdown in Disordered Solids*, ed. AK Sen, KK Bardhan, BK Chakrabarti, *Lecture Notes in Physics*, Vol. 762, pp. 1–35. Berlin, Heidelberg: Springer
6. Kirilyuk A, Kimel AV, Rasing T. 2010. *Rev. Mod. Phys.* 82:2731–84
7. Basov DN, Averitt RD, van der Marel D, Dressel M, Haule K. 2011. *Rev. Mod. Phys.* 83:471–541
8. Orenstein J. 2012. *Phys. Today* 65:44–50
9. Aoki H, Tsuji N, Eckstein M, Kollar M, Oka T, Werner P. 2014. *Rev. Mod. Phys.* 86:779
10. Giannetti C, Capone M, Fausti D, Fabrizio M, Parmigiani F, Mihailovic D. 2016. *Adv. Phys.* 65:58–238
11. Mankowsky R, Först M, Cavalleri A. 2016. *Rep. Prog. Phys.* 79:064503
12. Basov DN, Averitt RD, Hsieh D. 2017. *Nat. Mater.* 16:1077–88
13. Cavalleri A. 2017. *Contemp. Phys.* 59:31–46
14. Sawa A. 2008. *Mater. Today* 11:28–36

15. Cario L, Vaju C, Corraze B, Guiot V, Janod E. 2010. *Adv. Mater.* 22:5193–97
16. Pan F, Gao S, Chen C, Song C, Zeng F. 2014. *Mater. Sci. Eng.: R: Rep.* 83:1–59
17. Shirley JH. 1965. *Phys. Rev.* 138:B979–87
18. Dunlap DH, Kenkre VM. 1986. *Phys. Rev. B* 34:3625–33
19. Sambe H. 1973. *Phys. Rev. A* 7:2203–13
20. Hänggi P. 1988. *Quantum Transport and Dissipation*, ed. T Dittrich, P Hänggi, G-L Ingold, B Kramer, G Schön, W Zwerger, pp. 249–86. Weinheim, Germ.: Wiley-VCH
21. Moskalets M, Büttiker M. 2002. *Phys. Rev. B* 66:205320
22. Grifoni M, Hänggi P. 1998. *Phys. Rep.* 304:229–354
23. Chu SI, Telnov DA. 2004. *Phys. Rep.* 390:1–131
24. Joura AV, Freericks JK, Pruschke T. 2008. *Phys. Rev. Lett.* 101:196401
25. Tsuji N, Oka T, Aoki H. 2008. *Phys. Rev. B* 78:235124
26. Oka T, Aoki H. 2008. *Phys. Rev. B* 78:241104
27. Tsuji N, Oka T, Aoki H. 2009. *Phys. Rev. Lett.* 103:047403
28. Heidrich-Meisner F, González I, Al-Hassanieh KA, Feiguin AE, Rozenberg MJ, Dagotto E. 2010. *Phys. Rev. B* 82:205110
29. Lee WR, Park K. 2014. *Phys. Rev. B* 89:205126
30. Mikami T, Kitamura S, Yasuda K, Tsuji N, Oka T, Aoki H. 2016. *Phys. Rev. B* 93:144307
31. Qin T, Hofstetter W. 2017. *Phys. Rev. B* 96:075134
32. Murakami Y, Tsuji N, Eckstein M, Werner P. 2017. *Phys. Rev. B* 96:045125
33. Murakami Y, Eckstein M, Werner P. 2018. *Phys. Rev. Lett.* 121:057405
34. Seetharam KI, Bardyn CE, Lindner NH, Rudner MS, Refael G. 2015. *Phys. Rev. X* 5:041050
35. Dehghani H, Oka T, Mitra A. 2014. *Phys. Rev. B* 90:195429
36. Babadi M, Knap M, Martin I, Refael G, Demler E. 2017. *Phys. Rev. B* 96:014512
37. Sentef MA, Kemper AF, Georges A, Kollath C. 2016. *Phys. Rev. B* 93:144506
38. Sentef MA. 2017. *Phys. Rev. B* 95:205111
39. Kennes DM, Wilner EY, Reichman DR, Millis AJ. 2017. *Nat. Phys.* 13:479
40. D'Alessio L, Rigol M. 2014. *Phys. Rev. X* 4:041048
41. Lazarides A, Das A, Moessner R. 2014. *Phys. Rev. E* 90:012110
42. D'Alessio L, Polkovnikov A. 2013. *Ann. Phys.* 333:19–33
43. Kuwahara T, Mori T, Saito K. 2016. *Ann. Phys.* 367:96–124
44. Mori T, Kuwahara T, Saito K. 2016. *Phys. Rev. Lett.* 116:120401
45. Abanin D, Roeck WD, Ho WW, Huveneers F. 2017. *Commun. Math. Phys.* 354:809–27
46. Ponte P, Chandran A, Papi Z, Abanin DA. 2015. *Ann. Phys.* 353:196–204
47. Weinberg P, Bukov M, D'Alessio L, Polkovnikov A, Vajna S, Kolodrubetz M. 2017. *Phys. Rep.* 688:1–35
48. Haldar Asmi MR, Das A. 2018. *Phys. Rev. B* 97:245122
49. Goldman N, Dalibard J. 2014. *Phys. Rev. X* 4:031027
50. Eckardt A. 2017. *Rev. Mod. Phys.* 89:011004
51. Hasan MZ, Kane CL. 2010. *Rev. Mod. Phys.* 82:3045–67
52. Qi XL, Zhang SC. 2011. *Rev. Mod. Phys.* 83:1057–110
53. Castro Neto AH, Guinea F, Peres NMR, Novoselov KS, Geim AK. 2009. *Rev. Mod. Phys.* 81:109–62
54. Armitage NP, Mele EJ, Vishwanath A. 2018. *Rev. Mod. Phys.* 90:015001
55. Yan B, Felser C. 2017. *Annu. Rev. Condens. Matter Phys.* 8:337–54
56. Imada M, Fujimori A, Tokura Y. 1998. *Rev. Mod. Phys.* 70:1039–263
57. Thouless DJ. 1983. *Phys. Rev. B* 27:6083–87
58. Rice MJ, Mele EJ. 1982. *Phys. Rev. Lett.* 49:1455–59
59. Kitagawa T, Berg E, Rudner M, Demler E. 2010. *Phys. Rev. B* 82:235114
60. Thouless DJ, Kohmoto M, Nightingale MP, den Nijs M. 1982. *Phys. Rev. Lett.* 49:405–8
61. Bukov M, D'Alessio L, Polkovnikov A. 2015. *Adv. Phys.* 64:139
62. Eckardt A, Anisimovas E. 2015. *New J. Phys.* 17:093039
63. Deutsch JM. 1991. *Phys. Rev. A* 43:2046–49
64. Reimann P, Kastner M. 2012. *New J. Phys.* 14:043020

65. Berges J, Borsányi S, Wetterich C. 2004. *Phys. Rev. Lett.* 93:142002
66. Calabrese P, Cardy J. 2006. *Phys. Rev. Lett.* 96:136801
67. Moeckel M, Kehrein S. 2008. *Phys. Rev. Lett.* 100:175702
68. Mori T, Ikeda TN, Kaminishi E, Ueda M. 2017. *J. Phys. B. 51:112001*
69. Mitra A. 2018. *Annu. Rev. Condens. Matter Phys.* 9:245–59
70. Casas F, Oteo JA, Ros J. 2001. *J. Phys. A: Math. Gen.* 34:3379
71. Mananga ES, Charpentier T. 2011. *J. Chem. Phys.* 135:044109
72. Pershan PS, van der Ziel JP, Malmstrom LD. 1966. *Phys. Rev.* 143:574–83
73. Mentink JH, Balzer K, Eckstein M. 2015. *Nat. Commun.* 6:6708
74. Bukov M, Kolodrubetz M, Polkovnikov A. 2016. *Phys. Rev. Lett.* 116:125301
75. Kitamura S, Oka T, Aoki H. 2017. *Phys. Rev. B* 96:014406
76. Claassen M, Jiang H-C, Moritz B, Devereaux TP. 2017. *Nat. Commun.* 8:1192
77. Oka T, Aoki H. 2009. *Phys. Rev. B* 79:081406
78. Kitagawa T, Oka T, Brataas A, Fu L, Demler E. 2011. *Phys. Rev. B* 84:235108
79. Kitagawa T, Berg E, Rudner M, Demler E. 2010. *Phys. Rev. B* 82:235114
80. Lindner NH, Refael G, Galitski V. 2011. *Nat. Phys.* 7:490–95
81. Ishikawa T, Sagae Y, Naitoh Y, Kawakami Y, Itoh H, et al. 2014. *Nat. Commun.* 5:5528
82. Haldane FDM. 1988. *Phys. Rev. Lett.* 61:2015–18
83. Aharonov Y, Anandan J. 1987. *Phys. Rev. Lett.* 58:1593–96
84. Berry MV. 1984. *Proc. R. Soc. A: Math., Phys. Eng. Sci.* 392:45–57
85. Jotzu G, Messer M, Desbuquois R, Lebrat M, Uehlinger T, et al. 2014. *Nature* 515:237–40
86. Rechtsman MC, Zeuner JM, Plotnik Y, Lumer Y, Podolsky D, et al. 2013. *Nature* 496:196–200
87. Wang YH, Steinberg H, Jarillo-Herrero P, Gedik N. 2013. *Science* 342:453–57
88. Torres M, Kunold A. 2005. *Phys. Rev. B* 71:115313
89. Dehghani H, Oka T, Mitra A. 2015. *Phys. Rev. B* 91:155422
90. Oka T, Aoki H. 2010. *J. Phys.: Conf. Ser.* 334:5
91. Ikebe Y, Morimoto T, Masutomi R, Okamoto T, Aoki H, Shimano R. 2010. *Phys. Rev. Lett.* 104:256802
92. Gu Z, Fertig HA, Arovas DP, Auerbach A. 2011. *Phys. Rev. Lett.* 107:216601
93. Žutić I, Fabian J, Das Sarma S. 2004. *Rev. Mod. Phys.* 76:323–410
94. Kimel AV, Kirilyuk A, Usachev PA, Pisarev RV, Balbashov AM, Rasing T. 2005. *Nature* 435:655–57
95. Stanciu CD, Hansteen F, Kimel AV, Kirilyuk A, Tsukamoto A, et al. 2007. *Phys. Rev. Lett.* 99:047601
96. Tokura Y, Seki S, Nagaosa N. 2014. *Rep. Prog. Phys.* 77:076501
97. Tanabe Y, Moriya T, Sugano S. 1965. *Phys. Rev. Lett.* 15:1023–25
98. Katsura H, Nagaosa N, Balatsky AV. 2005. *Phys. Rev. Lett.* 95:057205
99. Sato M, Sasaki Y, Oka T. 2014. arXiv:1404.2010
100. Sato M, Takayoshi S, Oka T. 2016. *Phys. Rev. Lett.* 117:147202
101. Takayoshi S, Aoki H, Oka T. 2014. *Phys. Rev. B* 90:085150
102. Takayoshi S, Sato M, Oka T. 2014. *Phys. Rev. B* 90:214413
103. Kaminski A, Nazarov YV, Glazman LI. 2000. *Phys. Rev. B* 62:8154–70
104. Goldin Y, Avishai Y. 2000. *Phys. Rev. B* 61:16750–72
105. Kugel KI, Khomskiĭ DI. 1982. *Sov. Phys. Usp.* 25:231–56
106. Eckstein M, Mentink JH, Werner P. 2017. arXiv:1703.03269
107. Chaloupka J, Jackeli G, Khaliullin G. 2010. *Phys. Rev. Lett.* 105:027204
108. Bhattacharjee S, Lee SS, Kim YB. 2012. *N. J. Phys.* 14:073015
109. Kitaev A. 2006. *Ann. Phys.* 321:2–111
110. Bauer B, Cincio L, Keller BP, Dolfi M, Vidal G, et al. 2014. *Nat. Commun.* 5:5137
111. Shimizu Y, Miyagawa K, Kanoda K, Maesato M, Saito G. 2003. *Phys. Rev. Lett.* 91:107001
112. Koshihara S, Tokura Y, Mitani T, Saito G, Koda T. 1990. *Phys. Rev. B* 42:6853–56
113. Koshihara S, Tokura Y, Takeda K, Koda T. 1992. *Phys. Rev. Lett.* 68:1148–51
114. Cavalleri A, Tóth C, Siders CW, Squier JA, Ráksi F, et al. 2001. *Phys. Rev. Lett.* 87:237401
115. Yu G, Lee CH, Heeger AJ, Herron N, McCarron EM. 1991. *Phys. Rev. Lett.* 67:2581–84
116. Iwai S, Ono M, Maeda A, Matsuzaki H, Kishida H, et al. 2003. *Phys. Rev. Lett.* 91:057401

117. Perfetti L, Loukakos PA, Lisowski M, Bovensiepen U, Eisaki H, Wolf M. 2007. *Phys. Rev. Lett.* 99:197001
118. Wall S, Brida D, Clark SR, Ehrke HP, Jaksch D, et al. 2010. *Nat. Phys.* 7:114–18
119. Strohmaier N, Greif D, Jördens R, Tarruell L, Moritz H, et al. 2010. *Phys. Rev. Lett.* 104:080401
120. Fausti D, Tobey RI, Dean N, Kaiser S, Dienst A, et al. 2011. *Science* 331:189–91
121. Hu W, Kaiser S, Nicoletti D, Hunt CR, Gierz I, et al. 2014. *Nat. Mater.* 13:705–11
122. Kaiser S, Hunt CR, Nicoletti D, Hu W, Gierz I, et al. 2014. *Phys. Rev. B* 89:184516
123. Tokura Y, Okamoto H, Koda T, Mitani T, Saito G. 1988. *Phys. Rev. B* 38:2215–18
124. Asamitsu A, Tomioka Y, Kuwahara H, Tokura Y. 1997. *Nature* 388:50–52
125. Taguchi Y, Matsumoto T, Tokura Y. 2000. *Phys. Rev. B* 62:7015–18
126. Guiot V, Cario L, Janod E, Corraze B, Phuoc VT, et al. 2013. *Nat. Commun.* 4:1722
127. Hirori H, Shinokita K, Shirai M, Tani S, Kadoya Y, Tanaka K. 2011. *Nat. Commun.* 2:594
128. Oka T, Arita R, Aoki H. 2003. *Phys. Rev. Lett.* 91:066406
129. Oka T, Aoki H. 2005. *Phys. Rev. Lett.* 95:137601
130. Freericks JK, Turkowski VM, Zlatić V. 2006. *Phys. Rev. Lett.* 97:266408
131. Takahashi A, Itoh H, Aihara M. 2008. *Phys. Rev. B* 77:205105
132. Oka T, Aoki H. 2010. *Phys. Rev. B* 81:033103
133. Tsuji N, Oka T, Werner P, Aoki H. 2011. *Phys. Rev. Lett.* 106:236401
134. Oka T. 2012. *Phys. Rev. B* 86:075148
135. Bukov M, Kolodrubetz M, Polkovnikov A. 2016. *Phys. Rev. Lett.* 116:125301
136. Heisenberg W, Euler H. 1936. *Z. Phys.* 98:714–32. (Translated to English in arXiv:0605038)
137. Schwinger J. 1951. *Phys. Rev.* 82:664–79
138. Dunne GV. 2009. *Eur. Phys. J. D* 55:327–40
139. Gelis F, Tanji N. 2016. *Prog. Part. Nuclear Phys.* 87:1–49
140. Resta R. 1994. *Rev. Mod. Phys.* 66:899–915
141. King-Smith RD, Vanderbilt D. 1993. *Phys. Rev. B* 47:1651–54
142. Stafford CA, Millis AJ. 1993. *Phys. Rev. B* 48:1409–25
143. Liu M, Hwang HY, Tao H, Strikwerda AC, Fan K, et al. 2012. *Nature* 487:345–48
144. Fedotov AM, Narozhny NB, Mourou G, Korn G. 2010. *Phys. Rev. Lett.* 105:080402
145. Mayer B, Schmidt C, Grupp A, Bühler J, Oelmann J, et al. 2015. *Phys. Rev. B* 91:235113
146. Yamakawa H, Miyamoto T, Morimoto T, Terashige T, Yada H, et al. 2017. *Nat. Mater.* 16:1100–5
147. Mukai Y, Hirori H, Yamamoto T, Kageyama H, Tanaka K. 2016. *New J. Phys.* 18:013045
148. Knap M, Babadi M, Refael G, Martin I, Demler E. 2016. *Phys. Rev. B* 94:214504
149. Rozenberg MJ, Inoue IH, Sánchez MJ. 2004. *Phys. Rev. Lett.* 92:178302
150. Sow C, Yonezawa S, Kitamura S, Oka T, Kuroki K, et al. 2017. *Science* 358:1084–87
151. Silva REF, Blinov IV, Rubtsov AN, Smirnova O, Ivanov M. 2018. *Nat. Photonics* 12:266–70
152. Murakami Y, Eckstein M, Werner P. 2018. *Phys. Rev. Lett.* 121:057405
153. Martin I, Refael G, Halperin B. 2017. *Phys. Rev. X* 7:041008